Arabian Journal of Chemistry (2020) 13, 3889–3902

King Saud University

Arabian Journal of Chemistry

www.ksu.edu.sa
www.sciencedirect.com

ORIGINAL ARTICLE

Spectral characterization, electrochemical, antimicrobial and cytotoxic studies on new metal (II) complexes containing N_2O_4 donor hexadentate Schiff base ligand

Asma A. Alothman [a,*], Eida S. Al-Farraj [b], Wedad A. Al-Onazi [a], Zainab M. Almarhoon [a], Amal M. Al-Mohaimeed [a]

[a] *Department of Chemistry, College of Science, King Saud University, P.O. Box 22452, Riyadh 11495, Saudi Arabia*
[b] *Department of Chemistry, College of Science, Imam Mohammad Ibn Saud Islamic University (IMSIU), 11623 Riyadh, Saudi Arabia*

Received 13 January 2019; accepted 21 February 2019
Available online 28 February 2019

KEYWORDS

Electrochemical;
Schiff base metal(II) complexes;
Antimicrobial screening;
Cytotoxic activity

Abstract We report the biological activity of the new Schiff base ligand H_2L (H_2L = 6,6′-((1*E*,11*E*)-5,8-dioxa-2,11-diazadodeca-1,11-diene-1,12-diyl)bis(2,4-dichlorophenol)), its derived metal(II) complexes [Cu(L)] (1), [Co(L)] (2), [Ni(L)] (3) and [Zn(L)] (4), along with their structural characterizations by using various analytical and spectroscopic techniques. Electrochemical investigations showed that all of these Cu(II), Co(II) and Ni(II) complexes were reversibly reducible. Although the change of the number of unpaired electrons are different of the metal cations, they have an effect on the redox potentials of the Co(II)/(I), Ni(II)/(I) and Cu(II)/(I) couples. The ^{1}H NMR and FTIR data concluded that the Schiff base ligand H_2L acts as a hexadentate ligand coordinating with metal(II) ions through the oxygen atoms of the (—C—O—C), phenolic (—C—OH) groups and nitrogen atom of the azomethine (—CH=N—) group. UV-Visible absorption spectra studies clearly revealed the octahedral geometry of the prepared metal(II) complexes. Complexes 1 and 4 were found to be efficient in bringing about antimicrobial activities. The proposed mechanism of their antimicrobial activities has been discussed. 3-(4,5-Dimethylthiazol-2-yl)-2,5-diphenyltetrazolium bromide (MTT) assay showed the remarkable cytotoxicity of complex 1 (IC50 = 17 ± 1.3 μg/mL) on human breast cancer MCF-7 cells than Schiff base ligand H_2L and complexes 2–4. Moreover, AO/EB staining assay revealed cell death due to apoptosis in MCF-7 cells and

* Corresponding author.
E-mail address: aaalothman@ksu.edu.sa (A.A. Alothman).
Peer review under responsibility of King Saud University.

Production and hosting by Elsevier

https://doi.org/10.1016/j.arabjc.2019.02.003

the generation of ROS by the Schiff base ligand H_2L and its derived metal(II) complexes 1–4 may be a possible cause for their cytotoxic activity.

1. Introduction

Schiff bases are considered "privileged ligands" because they are easily prepared by the condensation between aldehyde and imines. The Schiff base ligands are able to coordinate with different metal ions, and to stabilize them in various oxidation states (Bayoumi et al., 2013). The Schiff base complexes have been used in catalytic reactions (Caselli et al., 2005). and as models for biological systems (Gomathi and Selvameena, 2012). Schiff bases are characterized by an imine group N═CH which helps to clarify the mechanism of Schiff transamination and racemization reaction in biological systems (Ritter et al., 2009). During the past two decades, considerable attention has been paid to the chemistry of metal complexes of Schiff bases containing nitrogen and other donors (Hasaninejad et al., 2018). Tetradentate Schiff bases with a N2O2 donor atom set are well known to coordinate with various metal ions, and this has attracted many authors (Kavitha and Anantha, 2019; Al-Adiwish et al., 2012; Sigmundova et al., 2008). The reactions of tetradentate Schiff bases derived from salicylaldehyde and diamine are the subject of many authors (Badr, 2001; Boghaei and Mohebi, 2002; Naeimi et al., 2007; Nayar and Ravikumar, 2014). These reactions are important due to great number of molecules that can be generated and the well-known ability of these tetradentate ligands to form stable complexes with different metal ions (Mizar and Myrboh, 2006). Symmetric tetradentate Schiff base complexes have been extensively used as macro cycle model (Kunta et al., 2017). Tetradentate Schiff base complexes have received considerable attention because of their potential uses as catalysts (Sutar, 2017), antibacterial (Aliyu and Zayyan, 2014), antifungal (Gandhi et al., 2017), antitumour agents (Sadeek et al., 2013). Moreover, recently we have reported a few Schiff base metal complexes including in Cu(II), Co(II) and Ni(II) complexes as potent cancer cell damaging metallodrugs (Li et al., 2014; Li and Yang, 2009). Among them, Cu(II) complexes showed better cytotoxic efficiency depending on their various ligand to metal coordination architectures.

Thus, the result of previous research works motivated us towards the synthesis of new

hexadentate Schiff base ligand H_2L and its derived [Cu(L)] (1), [Co(L)] (2), [Ni(L)] (3) and [Zn(L)] (4) complexes in order to evaluate their antimicrobial as well as cytotoxic activities. Their structural characteristics have been evaluated by various spectral and analytical techniques. Along with, their antimicrobial activity and cytotoxicity were also estimated *in vitro*.

2. Experimental section

2.1. Materials and characterization techniques

3, 5-dichloro salicylaldehyde, 1, 8-diamino-3, 6-dioxaoctane, acetate salts of metal(II), $Cu(OAc)_2{\cdot}2H_2O$, $Co(OAc)_2{\cdot}4H_2O$, $Ni(OAc)_2{\cdot}4H_2O$ and $Zn(OAc)_2{\cdot}2H_2O$ were purchased from Sigma Aldrich and used without further purification. Spectroscopic grade of solvents purchased from Merck and was used without additional purification process. ^{1}H NMR spectra were measured on a high-resolution Bruker 300 MHz spectrometer in DMSO d_6 solvent using TMS as the internal standard. The elemental analyses were determined using a Vario III CHN analyzer. Electronic absorption spectra were recorded using Shimadzu spectrometer 2500 PC series in the range 200–800 nm. FT-IR spectra were recorded using Shimadzu Fourier-Transform Infrared spectrometer. SEM images of some obtained products were taken in JEOL JSM-5200 LV equipment. TEM images were recorded using transmittance electron microscope (TEM-2100). EDX measurements wear carried out on Bruker XFlash.

2.2. Synthesis protocols

2.2.1. Synthesis of Schiff base ligand H2L

1, 8-diamino-3, 6-dioxaoctane (1.48 g, 10 mmol) was dissolved in ethanol (10 mL) and kept for stirring, to this solution 3, 5-dichloro salicylaldehyde (3.82 g, 20 mmol) was added drop wise and the reaction mixture was allowed to reflux for 3 h (Scheme 1). Then the completion of the reaction was checked by TLC and the product obtained from the reaction mixture was extracted with ethyl acetate and the desired product (Schiff base ligand H2L) was obtained as yellow coloured solid by evaporating the organic layer. Finally, the yellow coloured solid product washed in ice cold ethanol (15 mL) and dried *in vacuo* over anhydrous $CaCl_2$.

6,6′-((1E,11E)-5,8-dioxa-2,11-diazadodeca-1,11-diene-1,12-diyl)bis(2,4 dichloro-phenol) **(H_2L)**

Yield: 87%. M.F. ($C_{20}H_{20}Cl_4N_2O_4$); colour: Yellow; m.p. °C:182–184; Anal. cal. for [$C_{16}H_{15}N_3O_2$]: C, 68.31%; H, 5.37%; N, 14.94%, Found: C, 68.24%; H, 5.30%; N, 14.89%, FT-IR (KBr disc cm^{-1}): 1718 ν(—C═O), 1638 ν (—CH═N), 1619 ν(—C—O—C), ^{1}H NMR (DMSO d_6) (δ, ppm): 2.4 (s, 3H, C—CH_3), 3.1 (s, 3H, N—CH_3), 7.7–6.9 (m, 8, ArH & hetero-H), 8.3 (s, 1H, —CH═N); ^{13}C NMR (DMSO d_6) (δ, ppm): 10.3 (s, 1C, C—CH_3), 36.3 (s, 1C, N—CH_3), 55.2–136.7 (m, 13, Ar—C & hetero—C), 145.8 (s, 1C, —C—O—), 152.3 (s, 1C, C═O), 161.3 (s, 1C, —CH═N); ESI-MS: 281 (molecular ion peak).

2.2.2. Synthesis of metal(II) complexes 1–4

All metal(II) complexes 1–4 were prepared by using the following general procedure:

Ethanolic solution (20 mL) of Schiff base ligand H2L (0.4938 g, 1 mmol) and the appropriate metal(II) acetate salt (1 mmol) were mixed thoroughly *via* magnetic stirring and refluxed for 2 h, cooled to room temperature (Scheme 2). The resulting colored precipitate of meta(II) complexes was filtered, washed in the ice cold ethanol (15 mL) and dried *in vacuo* over anhydrous CaCl2.

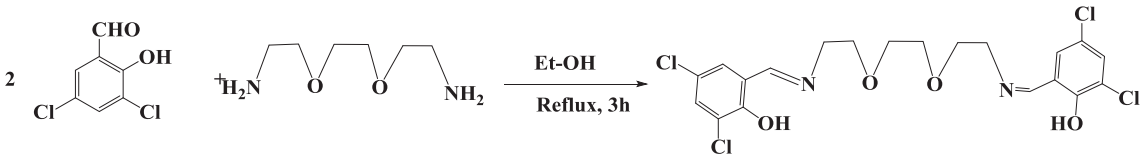

Scheme 1 Synthetic protocol of Schiff base ligand H_2L.

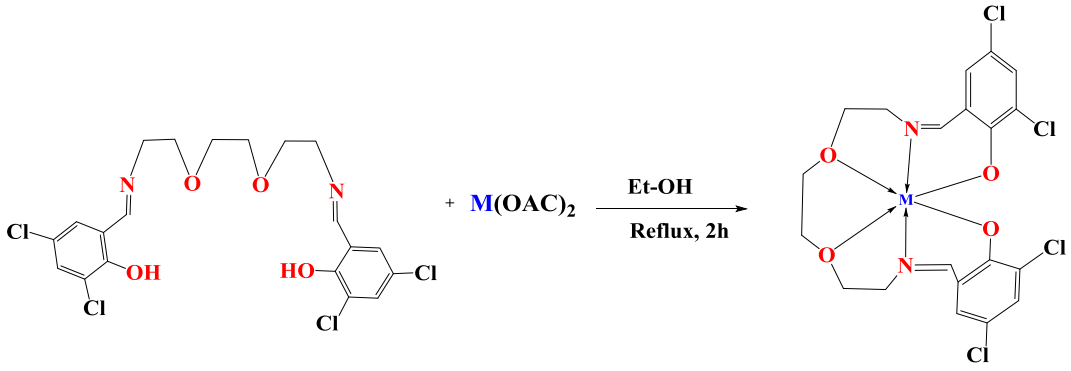

M = Cu(II) (1), Co(II) (2), Ni(II) (3) and Zn(II) (4)

Scheme 2 Synthetic protocol of metal(II) complexes 1–4.

2.3. In vitro antimicrobial studies

2.3.1. Antibacterial screening

Antibacterial activity of the Schiff base ligand H2L and its derived metal(II) complexes 1–4 were explored by the utilization of the agar well diffusion assay (Mathan Kumar et al., 2018). The antibacterial activity of the Schiff base ligand H2L and its derived metal(II) complexes 1–4 were studied against the *Escherichia coli*, *Staphylococcus aureus* and *Psuedomonas aeruginosa*, using the following protocol: DMSO solution of the appropriate compound 2 mg/ml of each compound (H2L and complexes 1–4) were prepared for antibacterial assay. Centrifuged pellets of bacteria containing about 10^4-10^6 CFU/mL were spread on the surface of Muller Hinton agar plates. Sterilized metallic bores were used to create walls in culture medium and the nutrients of agar media were added, before the nutrients were autoclaved and cooled down to 45 °C. After that, the agar medium was seeded with the 10 mL of prepared testing compound to have 10^6 CFU/mL. Finally, the antibacterial activity of the Schiff base ligand H2L and its derived metal(II) complexes 1–4 was determined by measuring the diameter of the inhibition zone (in mm) and the results compared with the standard drug Amoxicillin.

2.3.2. Antifungal screening

The inhibitory activity of the Schiff base ligand H2L and its derived metal(II) complexes 1–4 against the fungal species of *Aspergillus niger*, *Aspergillus flavus* and *Candida albicans* demonstrated by the paper disc method (Kesavan et al., 2017). In a typical procedure, DMSO solution (2 mg/mL) of the testing compound (H2L and complexes 1–4) was added to Potato Dextrose Sugar (PDA) culture medium in sterilized petri dishes and allowed to solidify. The filter paper discs with the diameter of the 5 mm were placed on nutrient culture medium mixed with appropriate fungal strains. Then these petri dishes were incubated at 37C for 48 h. Finally, radial growth inhibition diameter (in mm) of the Schiff base ligand H2L and its derived metal(II) complexes 1–4 over the control was calculated and compared with the standard drug of Ketoconazole.

2.4. In vitro cytotoxic studies

2.4.1. Cancer cell culture

The human breast cancer cells (MCF-7) were cultured in DMEM-F12 Ham supplemented with 10% fetal bovine serum, 100 µg/mL of penicillin, 100 µg/mL of streptomycin and 2.5 µg/Ml of amphotericin B. Cells were 96 well culture plates, at 37 °C under a humidified atmosphere of 5% CO2 in a CO2 incubator.

2.4.2. MTT cytotoxic assay

MTT (3-(4,5-dimethylthiazol-2-yl)-2,5-diphenyltetrazolium bromide) assay was demonstrated using previously described method (Dhahagani et al., 2018). In a classic method, DMSO solution (0–300 µM) of the Schiff base ligand H2L and its derived metal(II) complexes 1–4 were added to the wells containing 1×10^4 MCF-7 cells/well, moreover 200 µL of fresh culture medium was addedafter their seeding for 24 h. After that, 20 µL PBS solution of MTT solution (5 mg/mL) was added to each well and the plates were wrapped with aluminium foil and kept for incubation (4 h) at 37 °C. At the end of incubation, purple colored formazan product formed was dissolved by the addition of DMSO (100 µL) to each well. The absorbance was monitored at 570 (measurement) and 630 nm (reference) using 96 well plate reader. The assay was performed in triplicate and the data were plotted against the concentration of the testing compounds and the relative cancer

cell viability (%) in comparison to the control cells; from this the IC50 value (in μg/mL) of the Schiff base ligand H_2L and its derived metal(II) complexes 1–4 was evaluated.

2.4.3. AO/EB staining assay

AO/EB staining assay was performed to detect the morphological changes in apoptotic MCF-7 cancer cells treated with Schiff base ligand H_2L and its derived metal(II) complexes 1–4. Initially, MCF-7 cancer cells were incubated with Schiff base ligand H_2L and its derived metal(II) complexes 1–4 (25 μg/mL) for 24 h. Then 1 μg/mL of AO dye was added to each well and incubated for further 15 min in the dark place at 37 °C. After that, cancer cells were washed and again stained with EB (Dhahagani et al., 2018). The instant fluorescence images were captured with a Nikon Eclipse fluorescence microscope system.

3. Results and discussion

3.1. Spectroscopic and analytical characterization

Schiff base ligand H2L and its derived metal(II) complexes 1–4 were found to be highly coloured soluble in common solvents such as methanol, ethanol, DMSO, chloroform, acetonitrile and acetone. The analytical and magnetic measurement data of the Schiff base ligand H2L and its derived metal(II) complexes 1–4 are given in Table 1 and were in good agreement with their proposed molecular formula. The elemental analysis results of the metal(II) complexes 1–4 reveals the 1:1 ratio formation of the M(II) ions with the Schiff base ligand H2L (like ML form) as shown in Scheme 1. The molar conductance measurement of metal(II) complexes 1–4 was performed in DMSO solution (1×10^{-3} M) at room temperature, and were found to be 17–22 Ω^{-1} cm^2 mol^{-1}, supporting to their nonelectrolyte nature (Arun and Raman, 2014). (See Table 2.).

3.1.1. ^1H NMR spectra

^1H NMR spectra of the Schiff base ligand H2L and complex 4 were recorded in the DMSO d_6 solvent and the corresponding spectra are given in **Fig. S1**. The Schiff base ligand H2L shows singlet peak at 14.56 ppm for phenolic proton (—OH). A sharp peak at 8.50 ppm has been attributed to azomethine proton (—N=CH—) of the Schiff base ligand H2L. Moreover, its aromatic protons appear as a multiplet in the region of 7.37–7.56 ppm with J = 2.7 Hz indicates the presence of meta coupling of the protons. Methylene protons (N-CH2—) attached to azomethine nitrogen appears at 3.74 ppm with J = 4.8 Hz, as well as another methylene protons (—CH2—O) seems at 3.67 ppm with J = 4.8 Hz, indicating vicinal coupling of the protons. In the ^1H NMR spectrum of the complex 4 (compared with Schiff base ligand H2L), the peak due to the phenolic proton (—OH) is absent, while the peak due to the azomethine proton (—N=CH—) is shifted to 8.14 ppm, clearly indicates the involvement of the phenolic —OH and azomethine nitrogen atom in coordination with central metal(II) ion (Halli and Sumathi, 2012). Additionally, the peak of aromatic ring protons is shifted to 7.07–7.46 ppm. Moreover, the peaks of methylene protons of N-CH2— and —CH2—O are also shifted to deshielded region of 4.10 and 3.74, correspondingly. Thus, the formation of hexadentate Schiff base

Table 1 Physical, analytical, molar conductance and magnetic moment measurements of the Schiff base ligand H_2L and its derived metal(II) complexes 1–4.

Compound	Empirical formula [Mol. Wt.]	Colour [Yield]	Elemental Analysis Found (Calcd.) (%)					Magnetic moment (μ_{eff})	Λ_m [a] DMSO
			C	H	N	Cl	M		
H_2L	$C_{20}H_{20}Cl_4N_2O_4$ [494.2]	Yellow [87]	48.60 (48.61)	4.0.08 (4.08)	5.66 (5.67)	28.67 (28.69)	–	–	–
1	$C_{20}H_{18}Cl_4CuN_2O_4$ [555.7]	Green [76]	43.22 (43.23)	3.25 (3.26)	5.03 (5.04)	25.49 (25.52)	11.42 (11.43)	1.87	18
2	$C_{20}H_{18}Cl_4CoN_2O_4$ [551.1]	Brown [72]	43.59 (48.59)	3.29 (3.29)	5.07 (5.08)	25.73 (25.73)	10.69 (10.69)	3.83	17
3	$C_{20}H_{18}Cl_4NiN_2O_4$ [550.9]	Green [74]	43.61 (43.61)	3.28 (3.29)	5.07 (5.09)	25.72 (25.74)	10.65 (10.65)	2.87	22
4	$C_{20}H_{18}Cl_4ZnN_2O_4$ [557.6]	Yellow [68]	43.05 (43.08)	3.253.25)	5.00 (5.02)	25.44 (25.43)	11.72 (11.73)	Diamagnetic	19

[a] Λ_m = molar conductance (Ω^{-1} cm^2mol^{-1}).

Table 2 FT-IR spectral data of the Schiff base ligand H_2L and its derived metal(II) complexes 1–4 (in cm^{-1}).

Compound	ν(C═N)	ν(OH)	$\nu(C{-}O)_{phenolic}$	$\nu(C{-}O{-}C)_{ether}$	ν(M—O)	ν(M—N)
H_2L	1652 m[a]	3364br	1232 m	782 m	–	–
1	1622 m	–	1211 sh	708 s	512 m	410 m
2	1629 m	–	1208 m	693 s	526 w	406 m
3	1633 sh	–	1214 m	702 m	554 w	425 w
4	1624 m	–	1209 m	712 m	518 m	443 m

[a] sh = sharp, m = medium, br = broad, s = small, w = weak.

ligand H_2L and complex 4 with the proposed chemical structure was established.

3.1.2. FT-IR spectra

The FT-IR spectra of the Schiff base ligand H_2L and its derived metal(II) complexes 1–4 are depicted in **Fig. S2**. The spectrum of the free Schiff base ligand H_2L has showed a band in 1652 cm^{-1} region characteristics of the ν(C═N—) stretching mode indicating the successful formation of the hexadentate Schiff base H_2L as a product (Yadav et al., 2014). A broad band at 3364 cm^{-1} is observed due to phenolic—OH group that disappears in the spectra of all Schiff 's base metal(II) complexes suggest the deprotonation of phenolic—OH group by metal ion (Park et al., 2014). The bands observed at 1232 (Ammar et al., 2017) and 782 cm^{-1} (Buchner and Müller, 2018) are assigned to phenolic C—O and ether C—O—C stretching vibrations, respectively, which get shifted to lower frequency in all corresponding H_2L complexes and consistent with coordination via the protonated phenolic oxygen and ether oxygen, respectively. In favor of that, new bands due to ν(M—N) and ν(M—O) appear in the region of 406–443 cm^{-1} and 512–554, respectively (Al-Shaalan, 2011).

3.1.3. Electronic absorption spectra

The electronic absorption spectra of H_2L were experimentally recorded in the region of 200–650 nm at the room temperature and the concentration of 1.5×10^{-5} M in $CHCl_3$, THF, DCM, DMF and DMSO solvents **(Fig. S3)**. The absorption bands below300 nm in different organic solvents can be assigned to π-π* transitions of the azomethine (—HC═N—) group and aromatic benzene ring. The absorption bands observed in the range of 300–400 nm result from the n-π* transitions in azomethine and phenoxy groups of H_2L. Usually, the absorption bands appearing below 400 nm in the experimental UV spectrum of the 3,5-dichloro-2-hydroxy Schiff base derivative indicate the phenol-imine form, while the bands observed above 400 nm show the keto-amine form of the related molecule. Since the absorption band above 400 nm was not observed in the experimental UV–Vis spectrum for this study, it can be said that H_2L was in the form of phenol-imine in the selected organic solvents (Fig. 1).

The electronic absorption spectra of the metal(II) complexes 1–4 were recorded in chloroform at room temperature and the concentration of 1.5×10^{-5} M. Schiff base ligand H2L reveals three absorption maxima at 245 and 367 nm, which corresponds to π–π* and n–π* transitions respectively. Another one absorption maxima at 447 nm may occur due to intramolecular charge transfer within the whole structure of the Schiff base ligand H2L. Notably, absorption maxima correspond to π–π* and n–π* for complexes 1–4 **(**Fig. 2**)** shifted to the region of 238–249 nm and 273–348 nm, respectively with low extinction coefficient values. Besides the band for intramolecular charge-transfer transitions of Schiff base ligand H2L disappeared. The new bands in the region of 380–455 nm are due to LMCT transitions of complexes 1–4. These absorption bands clearly point out that, the octahedral geometry with slight distortion (Drago, 1991).

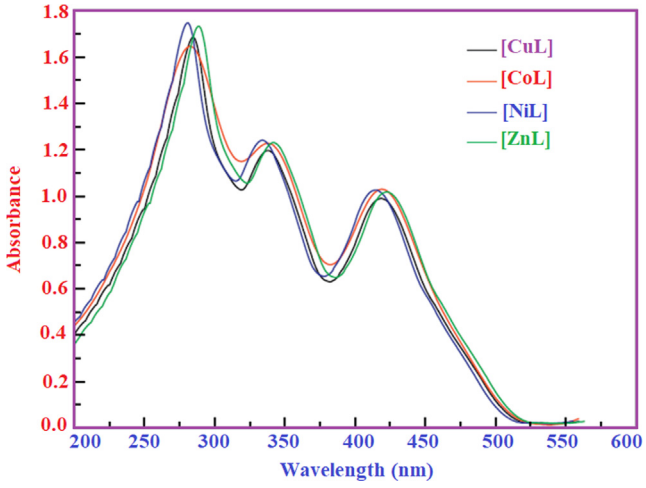

Fig. 2 UV–Vis. spectra of metal(II) complexes (1–4).

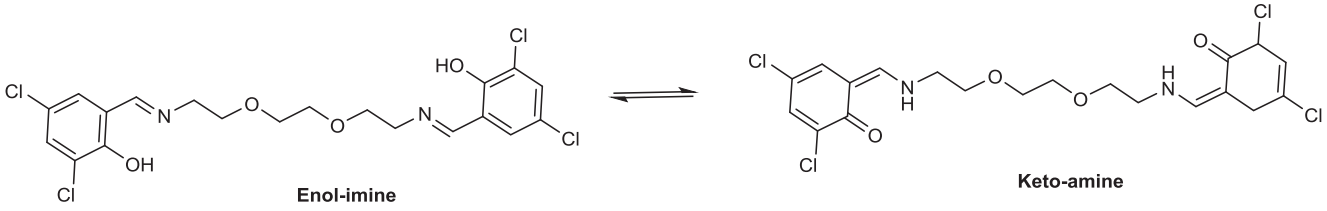

Fig. 1 Proposed structure oh H_2L ligand.

Table 3 Electrochemical[a] data of the reported Co(II), Ni(II)and Cu(II) complexes.

Complex	Electrochemical parameters			
	E_{pa} (V)	E_{pc} (V)	Δ_{Ep}[a] (V)	$E_{1/2}$[b] (V)
[CuL]	−0.783	−0.983	0.200	−0.883
[CoL]	−0.725	−0.960	0.235	−0.845
[NiL]	−0.669	−0.887	0.218	−0.777

[a] Supporting electrolyte $[NBu_4]ClO_4$ (0.1 M); scan rate, 100 mV/S; reference electrode Ag/AgCl; $\Delta_{Ep} = E_{pa}–E_{pc}$.
[b] $E_{1/2} = 1/2$ (Epa + Epc).

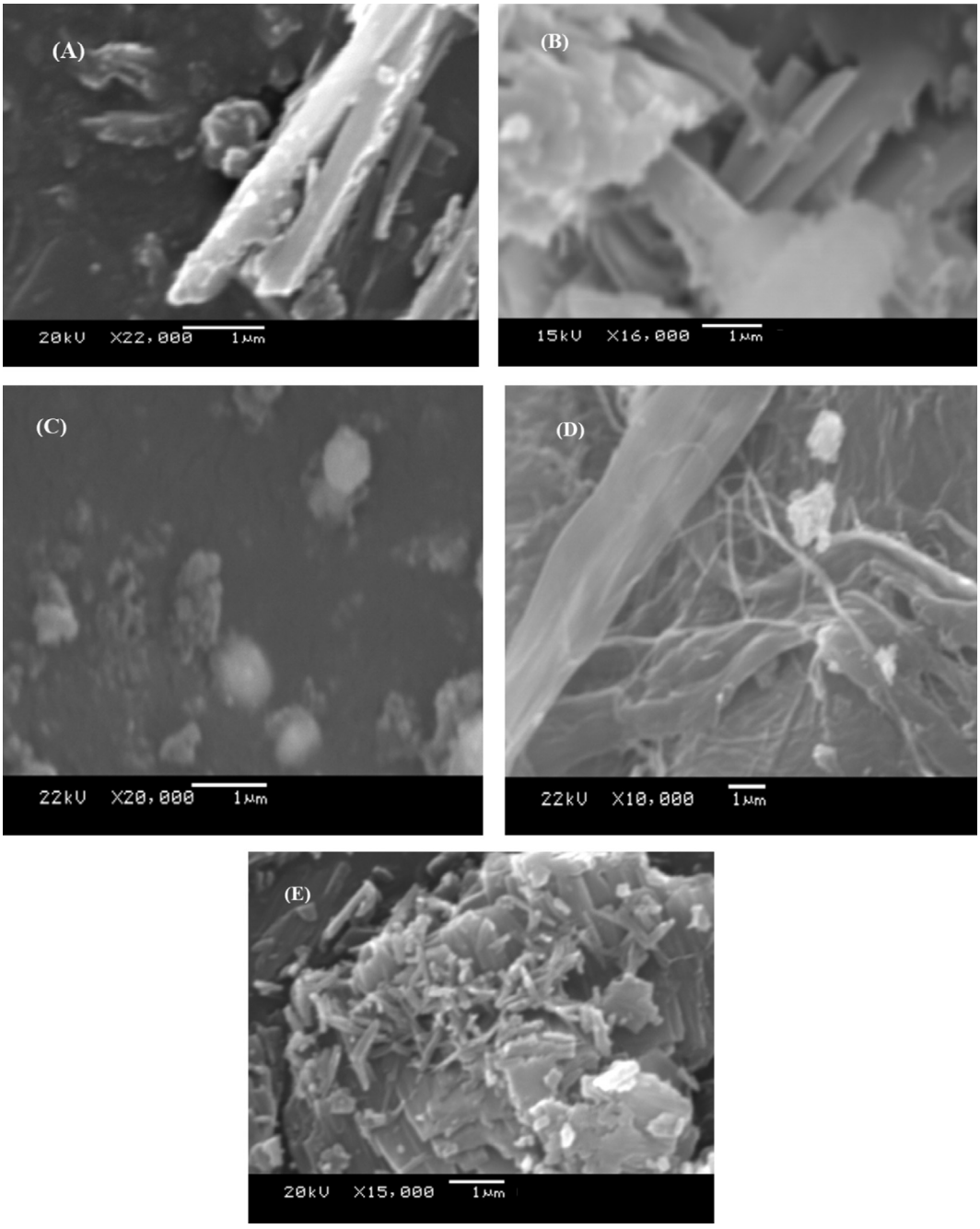

Fig. 3 SEM images of H_2L ligand and its metal (II) complexes (a–e), respectively.

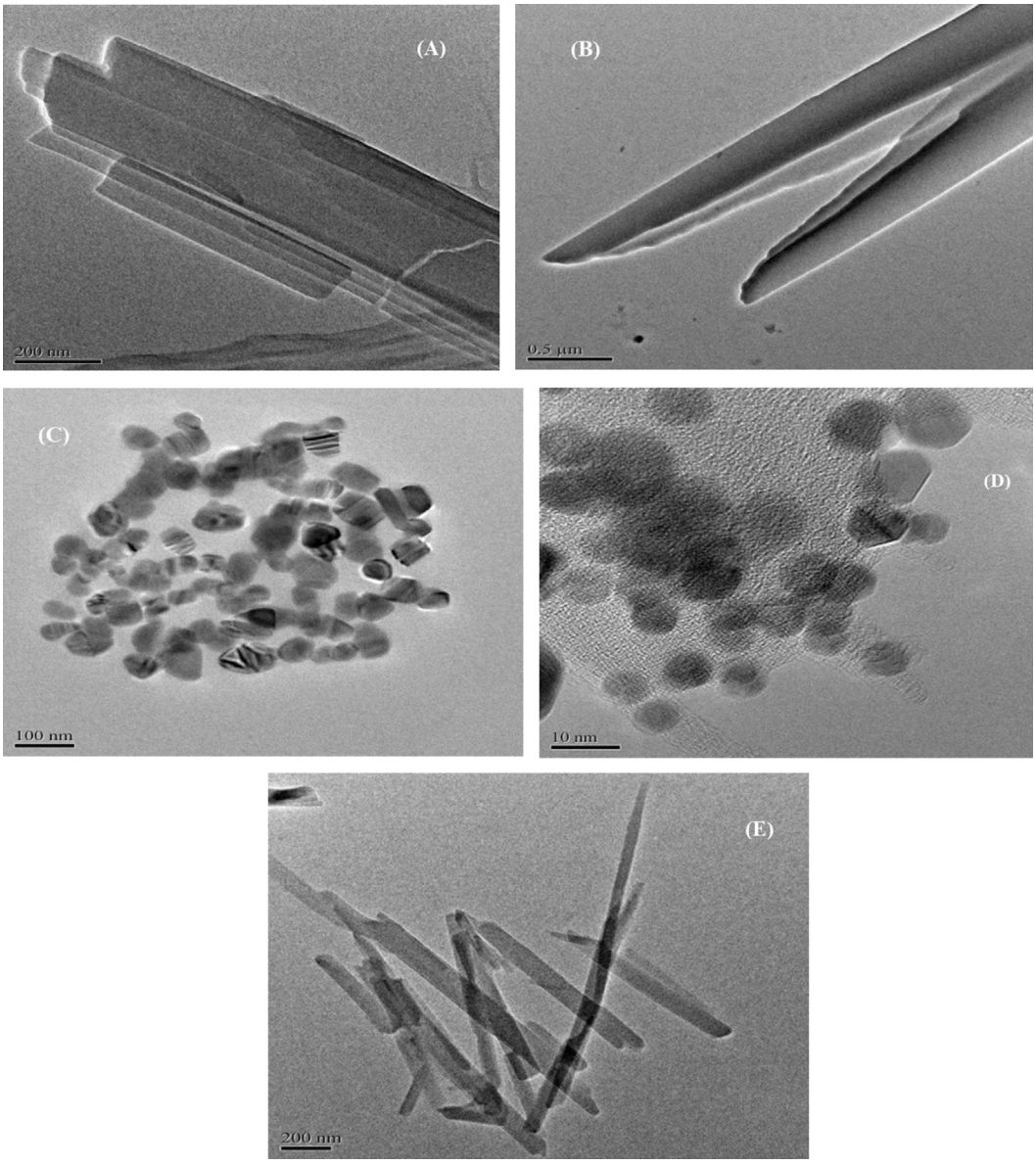

Fig. 4 TEM images of H_2L ligand and its metal (II) complexes (a–e), respectively.

3.2. Electrochemical study

The cyclic voltammetric studies of the M(II) complexes were carried out in acetonitrile solution, in the range +2.0 to −2.0 V using glassy carbon electrode as working electrode, Ag/AgCl as reference electrode and tetrabutyl ammonium chloride (0.1 M) as supporting electrolyte. The solution was deareated with a continuous flow of nitrogen gas for 15 min. before scanning. A respective voltammogram of the complex Cu has been depicted in **Fig. S4** and the data are given in Table 3. All the complexes are electroactive only with respect to metal center. The complexes (10^{-3} M) gave only quasi reversible electrochemical response due to M(II)–M(I) couple in the range of $E_{1/2}$ = −0.883 to −0.776 V, with peak to peak separation (Δ_{Ep}) of 0.195–0.240 V. This is attributed to slow electron transfer and adsorption of the complexes onto the electrode surface (Hosseini-Yazdi et al., 2015). The E_{12} and Δ_{Ep} values are in good agreement with those recently reported for other similar M(II) Schiff base complexes (Hosseini-Yazdi et al., 2015; Ramana et al., 2010). The E_{12} (reduction) values of the complexes containing one phenyl ring in the aldehyde part of the Schiff base ligands range from 0.52 to 0.63 V (Reynolds et al., 1988). When these values are compared with that of new complexes, it has been observed that the addition of one phenyl ring in the ligand causes positive shift in the E_{12} (reduction) values. This can be explained by the fact that the additional phenyl ring of electron withdrawing nature decreases the electron density around the metal center. It is not a question here

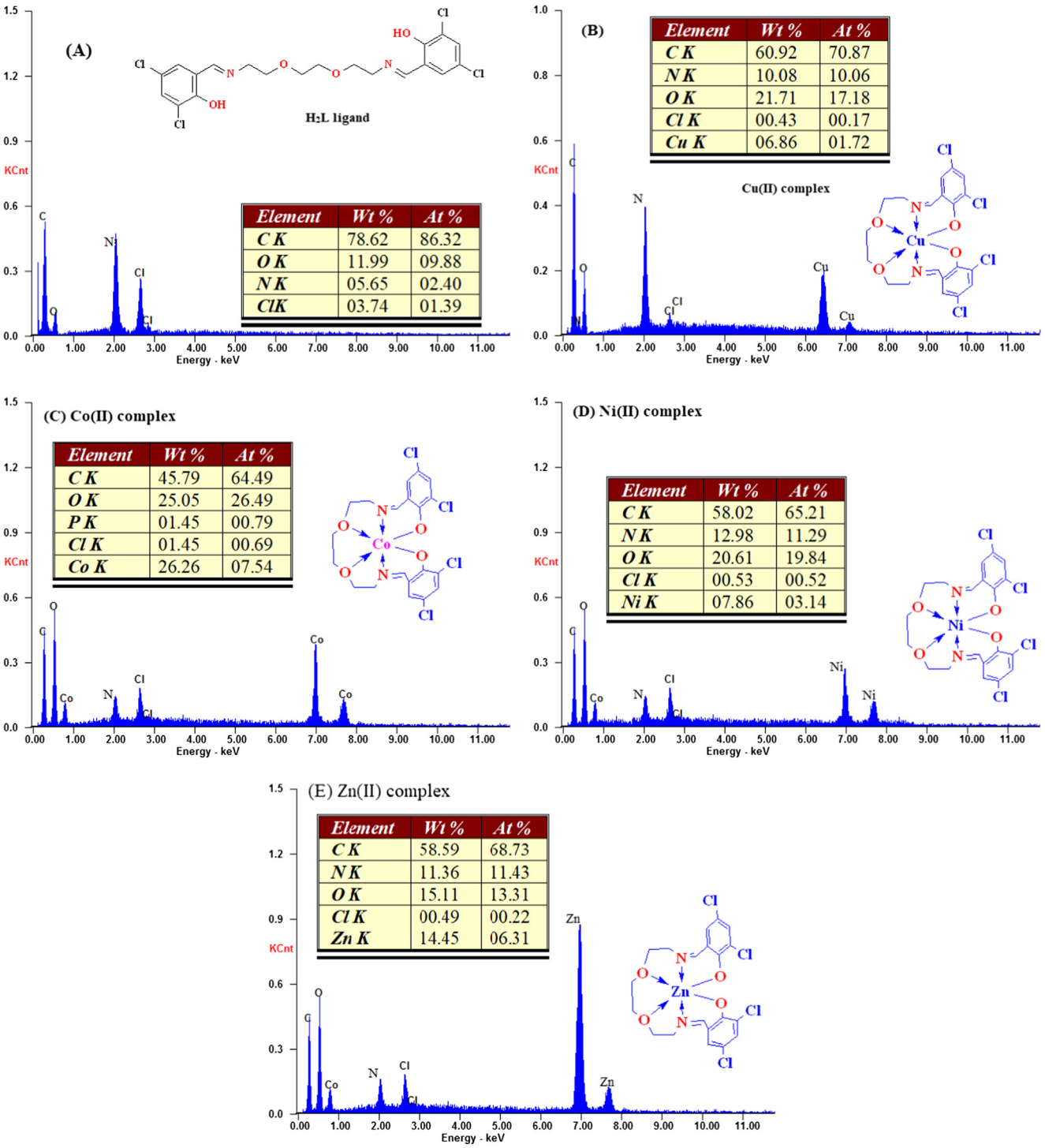

Fig. 5 EDX images of H_2L ligand and its metal (II) complexes (a–e), respectively.

of making an exhaustive study, for this it is necessary to vary several experimental parameters such as: the concentration, the speed of sweep of the field of study … etc. However, we have set ourselves the objective of highlighting the presence of the central ions in the complexes that we have synthesized, by identifying the wave or waves of the complexes, whose origin is the ion. More concretely, for each synthesized complex, we studied its electrochemical signal, which is compared to the recorded signals of two different solutions, one containing the ligand and the other containing the ion. The voltammograms recorded and reported on the Fig. S4 suggest the following points:- during the half-cycle, all the traces have redox waves, having no equivalent, neither in potential nor current during the half-cycle return, and whatever the redox species studied, this indicates that these compounds exhibit irreversible charge transfer; - in the potential range of −0.21 to −0.73 V, each

Table 4 Antibacterial screening results of the Schiff base ligand H_2L and its derived metal(II) complexes 1–4.

Compound	Diameter of inhibition zone (mm)		
	Escherichia coli	*Staphylococcus aureus*	*Psuedomonas aeruginosa*
H_2L	10 ± 1.5	9 ± 1.0	10 ± 1.0
1	16 ± 1.0	18 ± 1.5	15 ± 1.5
2	11 ± 1.5	10 ± 1.0	11 ± 0.5
3	11 ± 1.0	11 ± 1.5	12 ± 1.0
4	15 ± 1.0	18 ± 1.0	14 ± 0.5
Amoxicillin	8 ± 1.0	7 ± 0.5	9 ± 0.5

Table 5 Antifungal screening results of the Schiff base ligand H_2L and its derived metal(II) complexes 1–4.

Compound	Diameter of inhibition zone (mm)		
	Aspergillus niger	*Aspergillus flavus*	*Candida albicans*
H_2L	11 ± 0.5	10 ± 0.5	10 ± 1.0
1	15 ± 1.0	19 ± 1.0	14 ± 0.5
2	12 ± 1.0	11 ± 1.5	11 ± 1.0
3	12 ± 1.0	13 ± 0.5	11 ± 1.0
4	15 ± 0.5	17 ± 0.5	13 ± 1.0
Ketoconazole	10 ± 1.0	10 ± 1.0	9 ± 0.5

studied complexes have one or two reduction waves. In the same potential range, the ion alone has a single wave, while the H_2L ligand alone does not. This indicates, unambiguously, the presence of the ion in the structure of the complexes.

3.3. SEM, TEM and EDX morphological studies

The SEM pictures of H_2L and its complexes are shown in Fig. 3a–e, respectively. The micrograph of H_2L ligand complexes indicates road shaped particles. The [CuL] complex shows ice rock structure. The [CoL] and [NiL] complexes ice balls structure on the other hands, The[ZnL] complex shows ice grains structure was present.

Fig. 4a–e shows the TEM images of H_2L and its metal(II) complexes, respectively. The uniformity and similarity in between the particle forms of synthesized Schiff base ligand and its metal(II) complexes, indicate that the existence of morphological phases have a homogeneous matrix.

Table 6 IC50 values of the Schiff base ligand H2L and its derived metal(II) complexes 1–4 against MCF-7 cancer cells.

Compound	IC50 (μg/mL)
H_2L	208 ± 7.8
1	17 ± 1.3
2	94 ± 2.6
3	82 ± 2.4
4	53 ± 2.3
Cyclophosphamide	132 ± 2.9

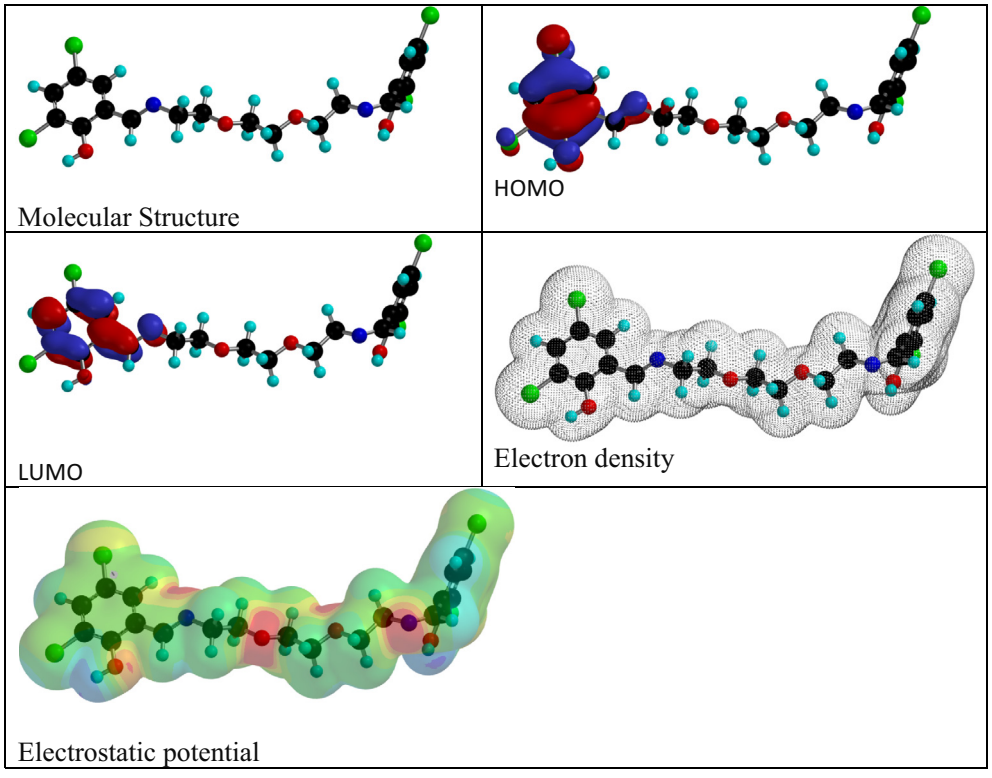

Fig. 6 The molecular structure, electron density, HOMO, LUMO and electrostatic potential of H_2L ligand.

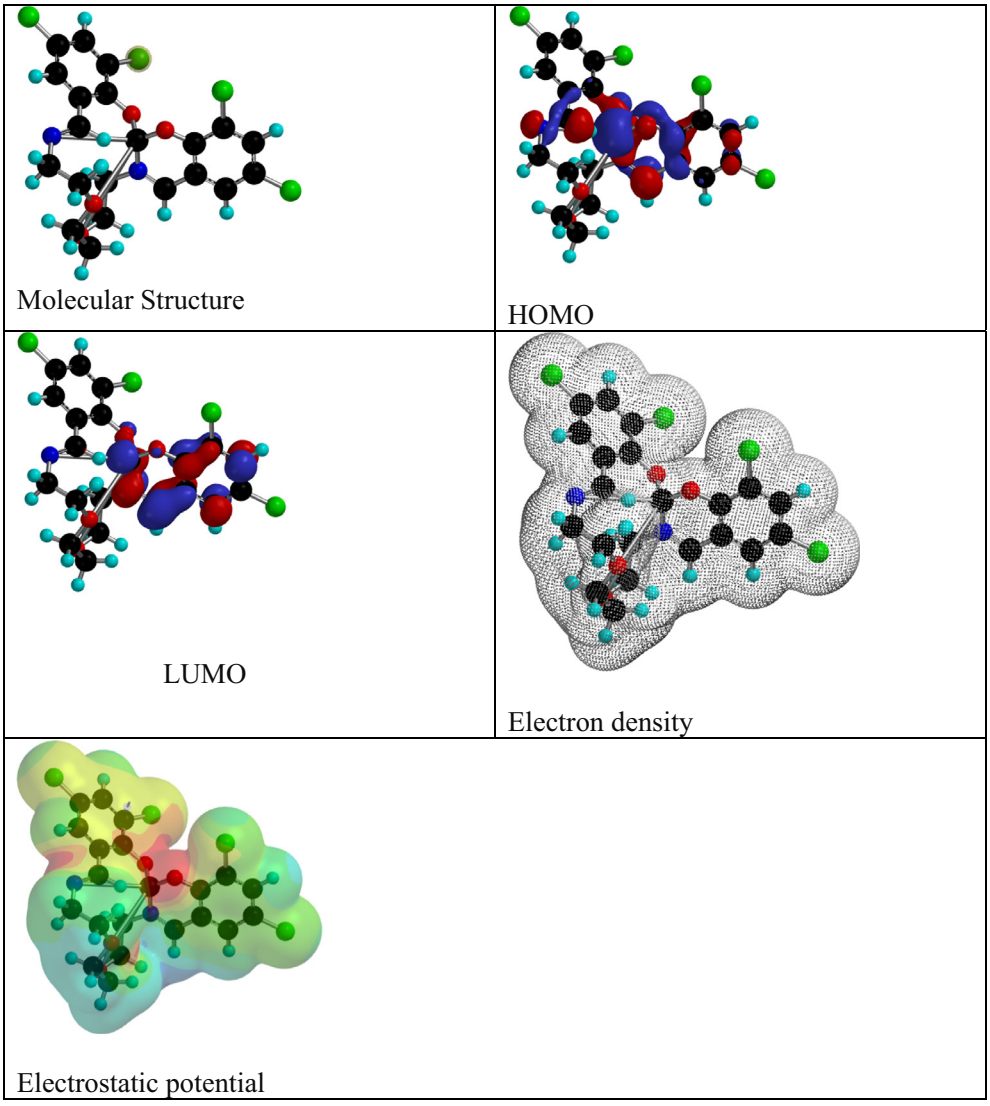

Fig. 7 The molecular structure, electron density, HOMO, LUMO and electrostatic potential of [CuL] complex.

The results by EDX have indicated that there are, H_2L ligand (carbon, chlorine, nitrogen and oxygen peaks) and copper, cobalt, nickel, zinc and carbon, nitrogen, chlorine and oxygen peaks, which meant there were carbon, chlorine, nitrogen and oxygen contamination or the deposited products were copper, cobalt, nickel, zinc oxides as shown in Fig. 5 a–e.

3.4. In vitro antimicrobial studies

3.4.1. Antibacterial activity

The antibacterial activity of Schiff base ligand H2L and its derived metal(II) complexes 1–4 were evaluated by agar well diffusion technique, in which the inhibit activity calculated as diameter of the inhibition zone (in mm). In the presence of Schiff base ligand H2L and its derived metal(II) complexes 1–4, the growth of bacterial species pointedly inhibited without the interruption of any other external agents. In mechanism, the formed ROS, as well as metal(II) ions, attack the negatively charged bacterial cell wall and cause cell wall leakage, resulting in the death of microbes (Cowley et al., 2002).

From the experimental observations, the antimicrobial activity against all the microbes was in the order of H2L < 3 < 2 < 4 < 1 (Table 4). The study reveals that complexes 1 and 4 inhibit the growth of bacteria stronger than others. This extended antibacterial activity was due to the maximum ROS (reactive oxygen species) production efficiency of Cu(II) and Zn(II) centred complexes 1 and 2, correspondingly. Remarkably, complexes 1 and 4 exposes extreme antibacterial activity on *Staphylococcus aureus* (18 ± 1.5 and 18 ± 1.0 mm correspondingly). Pointedly, synthesized Schiff base ligand H2L and its derived metal(II) complexes 1–4 exhibited better antibacterial activity than standard drug of Amoxicillin.

3.4.2. Antifungal activity

Both the Schiff base ligand H2L and its derived metal(II) complexes 1–4 reveals better antifungal activity, this may be due to

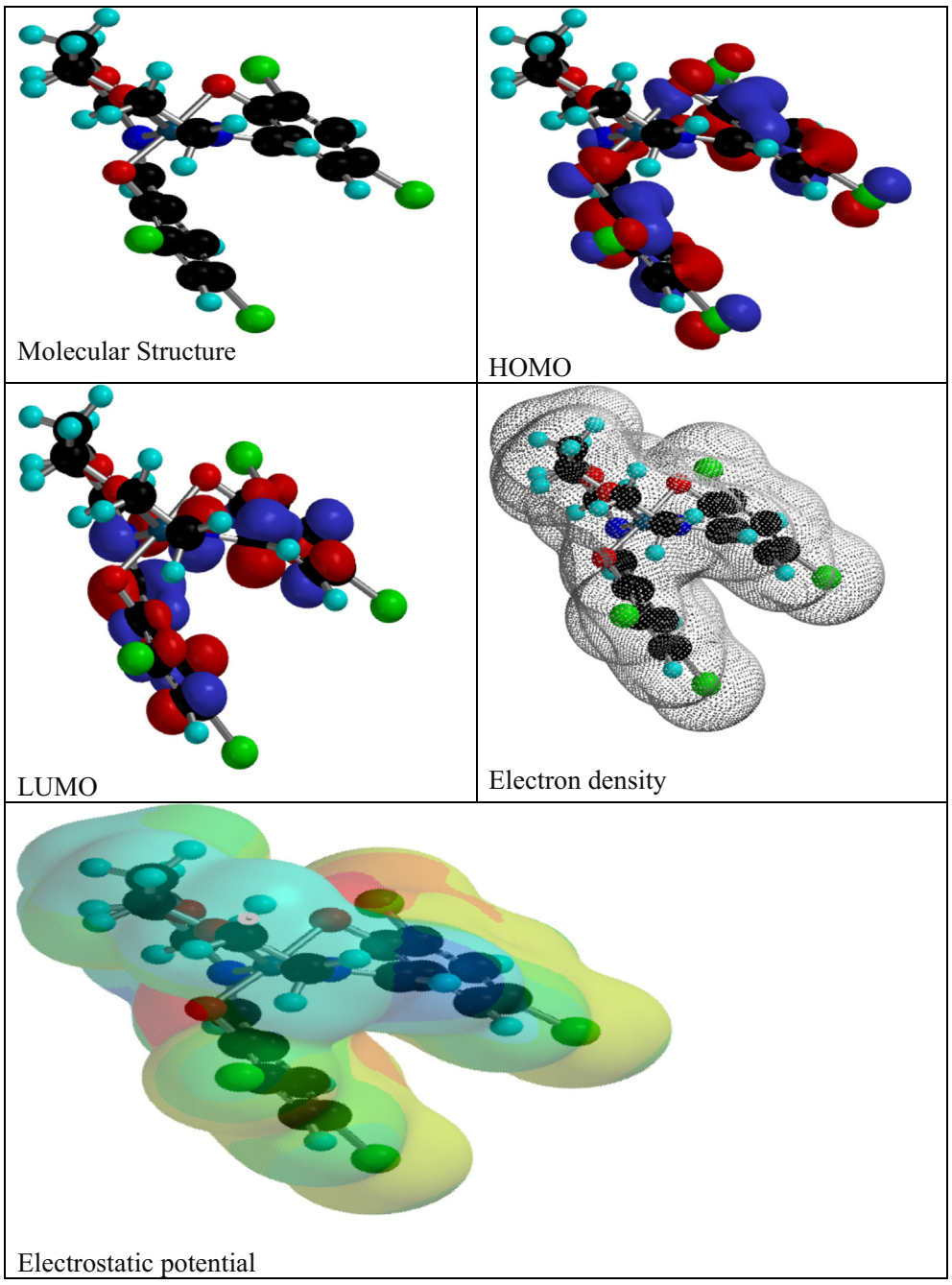

Fig. 8 The molecular structure, electron density, HOMO, LUMO and electrostatic potential of [CoL] complex.

the formation of ROS during the interaction of compound with biological oxygen molecules, thus the produced ROS effectively interacted with the membrane of the fungal species, inhibit their further growth and killed them (Qin et al., 2017). As a result, obtained from antibacterial screening, here also complexes 1 and 4 showed superior antifungal effect on all the tested fungus (especially on *Aspergillus flavus*) than standard drug of Ketoconazole (Table 5), due the same cause. Further, these results exhibit that complex 1 and 4 could be able to significantly inhibit the growth of microbes as good pharmacological agents.

3.5. In vitro cytotoxic studies

3.5.1. MCF-7 cancer cell viability study

Since Schiff base ligand H2L and its derived metal(II) complexes 1–4 showed better antimicrobial efficacy, it has been chosen for the further evaluation of *in vitro* cytotoxic activity with the MCF-7 cancer cells by MTT assay. The observed cytotoxicity (in terms of IC50) of the Schiff base ligand H2L and its derived metal(II) complexes 1–4 on MCF-7 cancer cell lines is illustrated in the Table 6. The present compounds were dissolved in DMSO and a blank sample solution containing

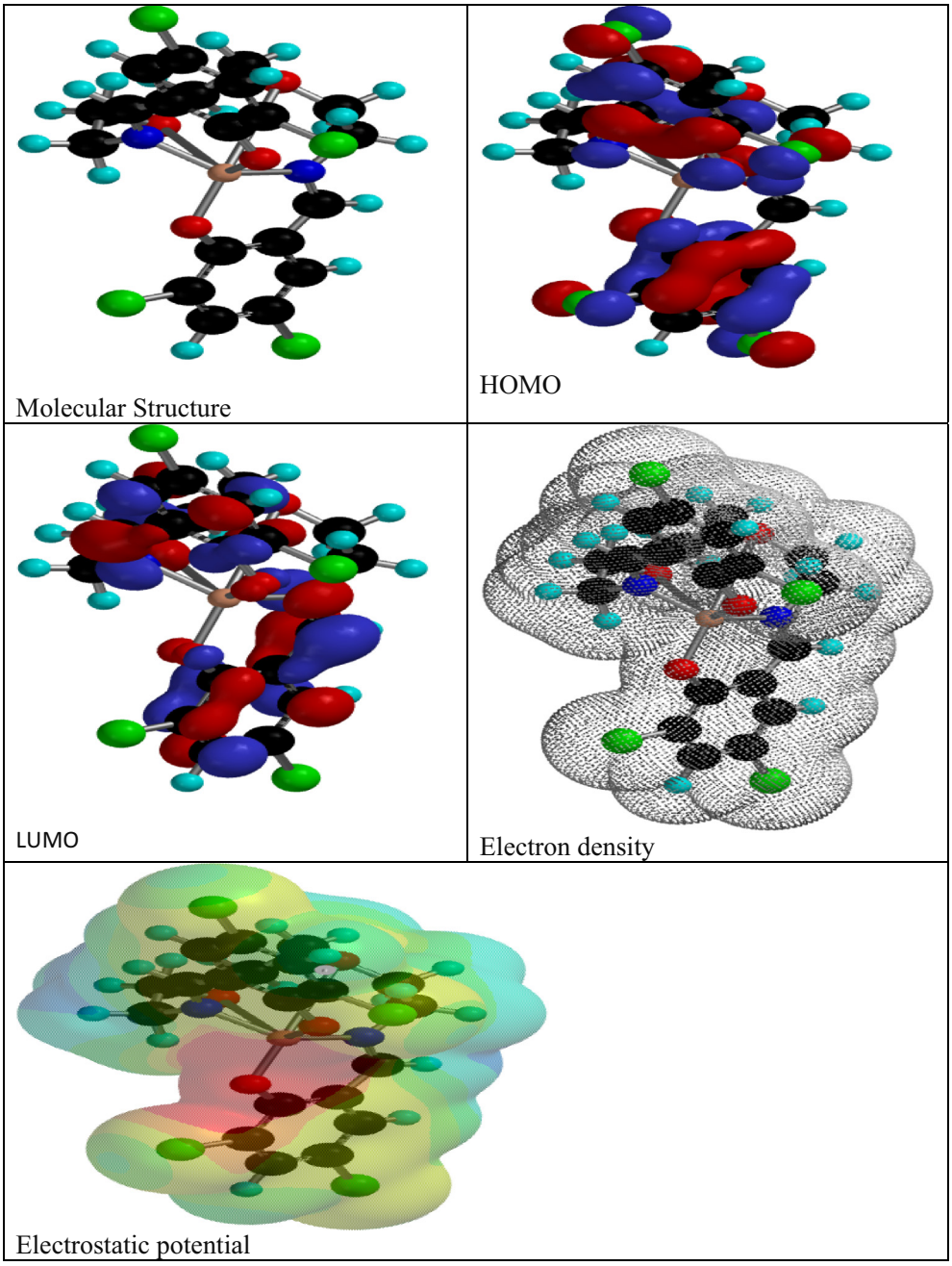

Fig. 9 The molecular structure, electron density, HOMO, LUMO and electrostatic potential of [ZnL] complex.

the same amount of DMSO was taken as the control to monitor the activity of the solvent alone in this experiment. The obtained results showed that complex 1 exhibited a higher cytotoxic effect on MCF-7 cancer cells (IC50 = 17 ± 1.3 μg/mL) than the H2L and complexes 2–4. The H2L and complexes 2–4 showed comparably larger IC50 values (208 ± 7.8, 94 ± 2.6, 82 ± 2.4 and 53 ± 2.3 μg/mL respectively) with a moderate cytotoxicity. According to the results, the high cytotoxicity of complex 1 was confirmed, its might due to strong stacking mode of interaction between the DNA bases of the cancer cells as well as extended ROS production efficacy (Usman et al, 2017).

3.5.2. Morphological and AO/EB staining studies

The molecular mechanism of cell death may occur *via* several mechanisms; among these apoptosis and necrosis are very common and it can be characterized by cell shrinkage, blebbing of plasma membrane, chromatin condensation and DNA fragmentation. Therefore the efficacy in inducing the cell death by Schiff base ligand H2L and its derived metal(II) complexes 1–4 have been evaluated using AO/EB staining-fluorescence microscopic technique (Fig. S5). In control cells, a uniform level of green fluorescence was observed in the nucleus, which illustrated the healthy live cancer cells, the cells which are treated with Schiff base ligand H2L did not lead any significant change on their morphological as well as fluores-

cence stain colour, while the treatment of metal(II) complexes 1–4 induced a significant amount of apoptosis on the MCF-7 cancer cells which may be occurred *via* two different ways; by showing a deep orange fluorescence in the cancer cells due to the early apoptosis and appeared as yellowish fluorescence with fragmented nucleus in the later apoptotic cells respectively. Therefore, it is concluded that the antitumor activities of these complexes 1–4 were triggered due to apoptosis instead of the necrosis pathway (Kesavan et al., 2018). Moreover, complex 1 efficiently killed the MCF-7 cancer cells than the others can be ascertained from the fluorescence images of apoptotic MCF-7 cancer cells. Since, complex 1 could be applied as a potent anticancer agent with significant antimicrobial properties.

3.6. Structures and quantum chemical calculations studies

In order to determine quantum chemical calculations, the coordination sites and make a comparison with the experimental observations, quantum chemical calculations of molecular structure, HOMO, LUMO, electron density and electrostatic potential have been carried out. Figs. 6–9 represents the optimized geometry of the ligand H_2L and its Cu(II), Co(II) and Zn(II) complexes as well as the charge density values calculated by the semiempirical method PM6 (Frisch et al., 2009). It has been found that the highest absolute values are those of the two protonated hydroxyl, two ether CH_2-O and two azomethine groups, suggesting that the latter's favor more chelation with the transition metals.

4. Conclusion

In summary, Schiff base ligand H2L and its derived Cu(II), Co (II), Ni(II) and Zn(II) complexes 1–4 were produced *via* facile synthesis strategy and their physico-chemical characteristics were confirmed by conventional spectroscopic and analytical techniques. UV-Visible absorption spectra studies clearly revealed the octahedral geometry of the prepared metal(II) complexes. The electrochemical behavior of these Cu(II), Co (II) and Ni(II) complexes leads us to conclude that the anodic peak potentials depend upon the nature of the equatorial Schiff base ligand. E_{pa} for different unpaired electrons changes according to the following trend: Cu > Co > Ni it means that unpaired electrons facilitate oxidation of the complex. In Co, there is an unpair electrons that is not very different from Ni and E_{pa} values confirm this fact. Also, the effect of the number of unpair electrons on anodic potentials is as follow: Ni < Co < Cu. The unpair electrons on Co and Ni are high unpaired electrons (three for Co(II) and two for Ni(II)), while unpair electrons on the Cu acts as low unpaired electrons by one unpair electron. The octahedral geometry of the complexes is confirmed using semiempirical method from PM6 calculations. Complexes 1 and 4 showed extended antimicrobial ability than the others, due to their higher ROS production efficacy. Besides that, complex 1 exhibited superier cytotoxic effect on MCF-7 cancer cells and the apoptosis mechanism for cancer cell assassination tracked by AO/EB stained fluorescence cell imaging study. We believe that, thus, complex 1 could be potentially used as an conventional anticancer agent, however, further extensive *in vivo* experiment is desirable to prove the anticancer efficacy.

Acknowledgment

This research project was supported by a grant from the "Research Center of the Female Scientific and Medical colleges", Deanship of Scientific Research, King Saud University.

Appendix A. Supplementary material

Supplementary data to this article can be found online at https://doi.org/10.1016/j.arabjc.2019.02.003.

References

Al-Adiwish, W., Yaacob, W., Adan, D., Nazlina, I., 2012. Int. J. Adv. Sci. Eng. Inf. Technol. 2, 27.
Aliyu, H., Zayyan, R., 2014. App. Sci. Report. 1, 445.
Al-Shaalan, N., 2011. Molecules 16, 8629.
Ammar, R., Alaghaz, A., Mohamed, E., Al-Bedair, L., 2017. J. Mol. Struct. 1141, 368.
Arun, T., Raman, N., 2014. Spectrochim. Acta A 127, 292.
Badr, S., 2001. Turk. J. Chem. 35, 131.
Bayoumi, H., Alaghaz, A., Aljahdali, M., 2013. Int. J. Electrochem. Sci. 8, 9399.
Boghaei, D., Mohebi, S., 2002. Tetrahedron 58, 5357.
Buchner, M., Müller, M., 2018. Z. Anorg. Allg. Chem. 644, 1186.
Caselli, A., Gallo, E., Ragaini, F., Oppezzo, A., Cenini, S., 2005. J. Organomet. Chem. 690, 2142.
Cowley, A., Dilworth, J., Donnelly, P., Labisbal, E., Sousa, A., 2002. J. Am. Chem. Soc. 124, 5270.
Dhahagani, K., Kesavan, M., Vinoth Kumar, G., Ravi, L., Rajagopal, G., Rajesh, J., 2018. Mater. Sci. Eng. C. 90, 119.
Drago, R., 1991. Physical Methods in Inorganic Chemistry. Affiliated East West, New Delhi.
Frisch, M., Trucks, G., Schlegel, H., Scuseria, G., Robb, J., Cheeseman, M., Montgomery, J., Vreven, T., Kudin, K., Burant, J., Millam, J., Iyengar, S., Tomasi, J., Barone, V., Mennucci, B., Cossi, M., Scalmani, G., Rega, N., Petersson, G., Nakatsuji, H., Hada, M., Ehara, M., Toyota, K., Fukuda, R., Hasegawa, J., Ishida, M., Nakajima, T., Honda, Y., Kitao, O., Nakai, H., Klene, M., Li, X., Knox, J., Hratchian, H., Cross, J., Bakken, V., Adamo, C., Jaramillo, J., Gomperts, R., Stratmann, R., Yazyev, O., Austin, A., Cammi, R., Pomelli, C., Ochterski, J., Ayala, P., Morokuma, K., Voth, G., Salvador, P., Dannenberg, J., Zakrzewski, V., Dapprich, S., Daniels, A., Strain, M., Farkas, O., Malick, D., Rabuck, A., Raghavachari, K., Foresman, J., Ortiz, J., Cui, Q., Baboul, A., Clifford, S., Cioslowski, J., Stefanov, B., Liu, G., Liashenko, A., Piskorz, P., Komaromi, I., Martin, R., Fox, D., Keith, T., Laham, A., Peng, C., Nanayakkara, A., Challacombe, M., Gill, P., Johnson, B., Chen, W., Wong, M., Gonzalez, C., 2009. Gaussian 09, Revision C.01. Gaussian, Inc., Willingford, CT.
Gandhi, S., Kumar, D., Tajudeen, S., Sheriff, A., 2017. Asian. J. Chem. 29, 1076.
Gomathi, V., Selvameena, R., 2012. Int. J. Sci. Res. 2, 24.
Halli, M.B., Sumathi, R.B., 2012. J. Mol. Str. 1022, 130.
Hasaninejad, A., Mojikhalifeh, S., Beyrati, M., 2018. Appl. Organomet. Chem. 32, 4380.
Hosseini-Yazdi, S., Hosseinpour, S., Khandar, A., Kassel, W., Piro, N., 2015. Inorg. Chim. Acta 427, 124.
Kavitha, N., Anantha, P.V., 2019. J. Mol. Str. 1176, 798.
Kesavan, M., Niranjan, G., Kotla, G., Ayyanaar, S., Vinoth Kumar, G., Rajagopal, G., Sivaraman, G., Webster, T., Rajesh, J., 2018. Nanomedicine NBM 14, 1643.
Kesavan, M., Vinoth Kumar, G., Dhaveethu Raja, J., Anitha, K., Karthikeyan, S., Rajesh, J., 2017. J. Photochem. Photobiol B: Bio. 167, 20.

Kunta, S., Guguloth, V., Chakilam, V., Vadde, R., 2017. J. Chem. Chem. Sci. 7, 1097.
Li, P., Niu, M., Niu, M., Hong, M., 2014. Z. Anorg. Allg. Chem. 640, 2238.
Li, Y., Yang, Z., 2009. Inorg. Chim. Acta. 362, 4823.
Mathan Kumar, S., Kesavan, M., Vinoth Kumar, G., Sankarganesh, M., Chakkaravarthi, G., Rajagopal, G., Rajesh, J., 2018. J. Mol. Struct. 1153, 1.
Mizar, P., Myrboh, B., 2006. Tetrahedron Lett. 47, 7823.
Naeimi, H., Safari, J., Heidarnezhad, A., 2007. Dyes and Pigments. 73, 251.
Nayar, C., Ravikumar, R., 2014. J. Coord. Chem. 67, 1.
Park, J., Kim, S., Kim, J., Chou, C., 2014. Org. Lett. 16, 178.
Qin, J., Shen, W., Chen, Z., Zhao, L., Qin, Q., Yu, Y., Liang, H., 2017. Sci. Rep. 7, 46056.
Ramana, N., Jeyamurugana, R., Sakthivela, A., Mitu, L., 2010. Spectrochimica Acta Part A 75, 88.
Reynolds, C., King, P., Richards, W., 1988. Nature 334, 80.
Ritter, E., Przybylski, P., Brzezinski, B., Bartl, F., 2009. Curr. Org. Chem. 13, 241.
Sadeek, S., El-Attar, M., Abd El-Hamid, S., 2013. J. Mol. Struct. 1051, 30.
Sigmundova, I., Zahradnik, P., Magdolen, P., Bujdakova, H., 2008. ARKIVOC Viii, 183.
Sutar, A., 2017. Int. J Mater. Sci. Appl. 2, 136.
Usman, M., Arjmand, F., Khan, R., Alsalme, A., Ahmad, M., Tabassum, S., 2017. RSC Adv. 7, 47920.
Yadav, M., Mishra, N., Sharma, N., Chandra, S., Kumar, D., 2014. Spectrochimica Acta Part A 132, 733.